A GIS-Based Transmissivity-Constrained Frequency Ratio Approach for Groundwater Potential Assessment in Basement Terrain

O. O. Oso[1, 2*], O. S. Ogungbemi [1], O. O. Afolabi [1], H. O. Aliu[3]

[1]Department of Geology, Afe Babalola University, Ado-Ekiti, Nigeria
[2]Department of Mineral & Petroleum Resources Engineering, Federal Polytechnic, Ado-Ekiti, Nigeria
[3]Department of Project & Contract Management, AUGJ Services Ltd, Bonny Island, Nigeria

ABSTRACT: Groundwater potential assessment in crystalline basement terrains is challenging due to heterogeneous subsurface conditions and limited recharge pathways. This study applied a transmissivity-constrained Frequency Ratio (FR) model within a Geographic Information System (GIS) framework to delineate groundwater potential zones (GPZs) in southwestern Nigeria. A total of 150 Vertical Electrical Sounding (VES) datasets were analyzed, of which 88 points with transmissivity >15 m²/d were considered hydraulically effective and used for model calibration. Twelve thematic layers—elevation, lithology, slope, drainage density, surface and subsurface lineament densities, geomorphology, curvature, topographic wetness index, soil texture, land use/land cover, and depth to fracture—were integrated to evaluate their influence on transmissivity. The FR analysis revealed that subsurface lineament density, lithology, and drainage density exerted the strongest control on transmissivity (FR > 2.5), indicating a high likelihood of groundwater occurrence in these classes. In contrast, steep slopes and high drainage density areas (FR < 1.0) showed limited groundwater potential. The resulting groundwater potential prediction map (GwPPM) classifies about 11.35% of the zone as very low potential, while 30.17%, 45.40% and 13.08% are categorized as low, moderate and high potential zones, respectively. Moderate-to-high potential zones, mainly around Igede-Ekiti and Iyin-Ekiti, correspond to highly fractured granitic terrains with gentle slopes and low drainage density. Validation with borehole yield data yielded ~80% accuracy, confirming model reliability. These results demonstrate that integrating transmissivity with FR-based GIS modeling provides an effective approach for groundwater assessment and supports sustainable exploration in basement terrains.

KEYWORDS: Frequency Ratio model; Transmissivity; GIS; Groundwater potential; Basement complex.

[Received Oct. 19, 2025; Revised Jun. 26, 2026; Accepted Jun. 28, 2026] Print ISSN: 0189-9546 | Online ISSN: 2437-2110

I. INTRODUCTION

Water is one of the most indispensable natural resources on Earth, serving as a foundation for both life and economic development. Among the different freshwater sources, groundwater remains the most reliable because it is less affected by seasonal variations and surface contamination. In many developing regions, especially in sub-Saharan Africa, groundwater serves as the principal source of supply for domestic, agricultural, and industrial use (MacDonald et al., 2012; Offodile, 2002). However, the limited understanding of subsurface conditions, particularly in crystalline basement terrains where aquifers are discontinuous and spatially variable hinders its sustainable development.

Crystalline basement terrains, which underlie a large part of West Africa, present one of the most challenging hydrogeological settings for groundwater exploration. Unlike sedimentary aquifers that are laterally extensive and porous, basement aquifers depend mainly on the extent of weathering and fracturing within otherwise impermeable rocks. These aquiferous zones are often localized and irregular, leading to significant differences in yield even within short distances (Adiat et al, 2020). As a result, an integrated approach that combines surface geomorphological indicators with subsurface geological and geophysical information is required to understand groundwater occurrence in such terrains. Drilling of boreholes randomly without this understanding often results in high failure rates and wasted resources.

Several interrelated factors influence groundwater storage and movement in basement terrains. These can be grouped into subsurface and surface conditions. Subsurface conditions such as the thickness of the weathered layer, fracture density, and depth to bedrock determine the ability of the aquifer to store and transmit water. On the surface, parameters including slope, elevation, soil type, drainage density, lineament density, and land use govern infiltration and recharge processes (Rahmati et al, 2015; Naghibi et al, 2016). Recognizing how these parameters interact to influence aquifer productivity is essential for efficient groundwater assessment and planning.

Transmissivity remains one of the most useful parameters for describing aquifer capacity owing to its ability to reflect how effectively groundwater can move through the saturated zone of an aquifer. Higher transmissivity generally indicates a

*Corresponding author: *osoolumuyiwa@yahoo.com*

doi: http://dx.doi.org/10.63746/njtd.v23i2.4130

more productive aquifer system. In basement terrains, transmissivity can be estimated from geoelectric parameters obtained through Vertical Electrical Sounding (VES), which provides information on subsurface resistivity and layer thickness. This method offers a cost-effective means of quantifying aquifer characteristics where direct pumping tests are not feasible (Adiat et al, 2020).

Although remote sensing and GIS-based methods have greatly advanced groundwater studies, many conventional models still rely on subjective weighting schemes such as the Analytical Hierarchy Process (AHP) or purely heuristic approaches that are not directly linked to field-derived hydrogeologic parameters. These limitations often reduce the predictive accuracy of the generated groundwater potential map. In contrast, probabilistic models such as the Frequency Ratio (FR) approach provide a more objective alternative by statistically relating actual aquifer parameters with spatially distributed groundwater-conditioning factors (Naghibi et al, 2016; Rahmati et al, 2015; Das and Pardeshi, 2018).

This study applies a transmissivity-constrained frequency ratio (TFR) model within a GIS framework to assess groundwater potential in a typical basement complex terrain. Transmissivity values derived from VES stations serve as the dependent variable, while twelve groundwater-influencing factors obtained from remote sensing and ancillary datasets act as independent variables. The approach quantifies the statistical relationship between these variables to produce a spatial distribution of groundwater potential zones (GPZs). The outcome of this research is expected to provide a more data-driven and objective framework for groundwater resource evaluation and sustainable management in crystalline basement terrains. This study advances groundwater potential modelling by integrating aeromagnetically derived subsurface lineament density into the Probabilistic Frequency Ratio (PFR) framework and by employing transmissivity as the response variable. Previous groundwater potential studies have largely relied on groundwater occurrence inventories and surface-derived conditioning factors (Jha et al., 2022; Ibrahim et al., 2024). By incorporating deep-seated structural information and a hydraulic parameter directly related to aquifer productivity, the present study provides a more hydrogeologically robust framework for groundwater potential assessment in crystalline basement terrains (Adiat et al., 2020; Osumeje et al., 2024).

II. THE STUDY AREA

A. Geographical Setting of the Study Area

The study area is situated in southwestern Nigeria and covers parts of Ekiti State, encompassing the towns of Iyin-Ekiti, Odo, Ilawe-Ekiti, Igbo Aso, Igede-Ekiti, and Orunro (Figure 1). Geographically, the area extends between latitudes 7°34′30″N and 7°40′30″N, and longitudes 5°05′00″E and 5°10′30″E, occupying a landscape characterized by gently undulating to moderately elevated terrain. The region is easily accessible through a network of major and minor roads that link the towns, while its proximity to Ado-Ekiti, the state capital, contributes to its socio-economic significance and growing human activities (Ojo et al, 2021; Ige et al, 2021).

Climatically, the study area lies within the humid tropical belt, experiencing two distinct seasons: the wet season, which lasts from April to October, and the dry season, which spans November to March. Mean annual rainfall ranges from about 1200 to 1500 mm, with average daily temperatures between 22°C and 32°C (Offodile, 2002; Ojo et al, 2021). Relative humidity is generally higher during the rainy season, enhancing infiltration and groundwater recharge (Adiat et al, 2020; Offodile, 1983). These climatic characteristics significantly influence the hydrologic regime of the area, particularly the depth and fluctuation of the water table within the weathered and fractured basement aquifers (Driscoll, 1986; Todd and Mays, 2005).

The drainage pattern is predominantly dendritic to sub-dendritic, indicating a relatively homogeneous lithology with subtle structural influences. Most of the streams are seasonal, flowing mainly during the wet months, which underscores the heavy dependence of local communities on groundwater resources for domestic and agricultural use (Offodile, 2002; Ojo et al, 2021). Land use across the area is diverse, comprising built-up residential settlements, cultivated farmlands, secondary forests, and patches of open grasslands. These surface features, in combination with slope gradients and soil characteristics, control surface runoff and infiltration dynamics, thereby influencing spatial variations in groundwater recharge potential across the terrain (Rahmati et al, 2015; Das and Pardeshi, 2018; Naghibi et al, 2016).

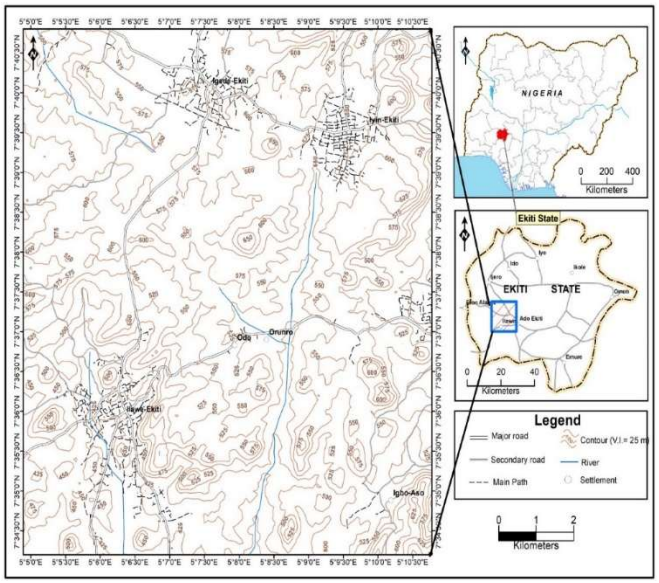

Figure 1 Topography map of the study area (Modified after NGSA, 2009)

B. Geological Setting of the Study Area

The study area lies within the southwestern part of Nigeria's Precambrian Basement Complex, a geologically heterogeneous terrain dominated by crystalline rock types. Key lithological units observed (Figure 2) include granite gneiss (OGp), charnockitic rocks (OGCh), quartzite and quartz schist (Qs), migmatite-gneiss (Mg), and fine- to coarse-grained granite (OGf). These belong to the migmatite–gneiss–quartzite complex, the older granite suite, and the charnockitic group—three principal divisions of the Nigerian Basement Complex (Offodile, 1983).

Among these, the migmatite-gneiss complex (Mg) is the most widespread in the area, especially around Ilawe-Ekiti. Its banded and foliated rocks are often heavily weathered and fractured, creating zones favorable for groundwater storage and movement. Accompanying belts of quartzite and quartz schist (Qs) provide enhanced recharge pathways, since fractured quartzite tends to retain secondary porosity and better resist weathering. Moving north and northeast toward Igede-Ekiti and Iyin-Ekiti, the terrain is underlain by porphyritic granite gneiss (OGp) of the older granite suite. Even though fresh granitic rock is typically impermeable, groundwater occurrence is common in its weathered mantle and along fractures, trends documented in basement complex aquifers elsewhere in Nigeria.

The OGf unit (fine- to coarse-grained granite), found in parts of the southeastern sector, generally has a more massive character. Yet, where weathering or tectonic deformation is pronounced, it can locally yield groundwater. A striking lithologic feature in the central zone, particularly around Odo and Orunro, is charnockitic rock (OGCh). These rocks are generally hard, less porous, and poorly permeable; however, where fractures or shear zones exist, modest groundwater reserves may occur (Adiat et al, 2020). Boreholes in such areas often yield poorly unless structural discontinuities are intersected.

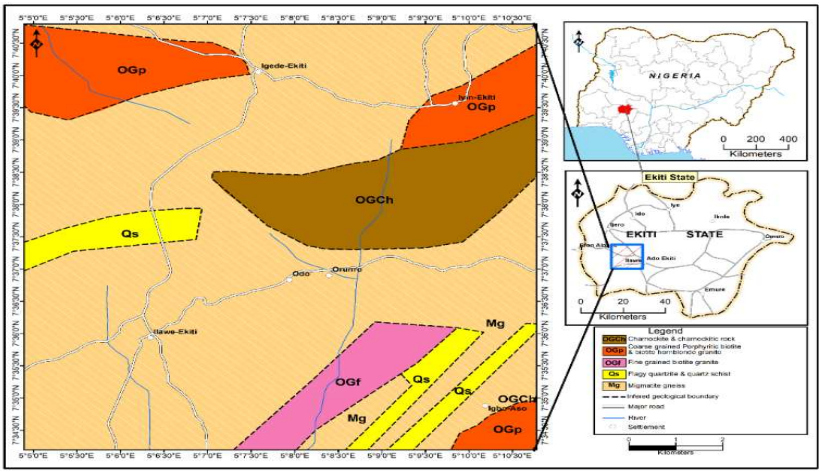

Figure 2 Geological map of the study area (Oso et al., 2026)

III. METHODOLOGY

This study integrates geophysical, remote sensing, and statistical approach to delineate GPZs in a crystalline basement terrain using a four-stage workflow involving: data acquisition, generation of thematic layers and evaluation of aquifer transmissivity, groundwater potential modeling using the Frequency Ratio (FR) technique, and validation of the derived GwPPM using borehole yield data.

A. Data Acquisition and Sources

The study integrated field-based geophysical measurements with remotely sensed and ancillary geospatial datasets. The primary data consist of 150 VES points collected across the study area using the Schlumberger configuration with a maximum current electrode separation (AB/2) of 100 meters. Aquifer transmissivity, which served as the dependent variable was subsequently estimated from the geoelectric parameters interpreted from these data. Secondary datasets including aeromagnetic, topographic, lithological, soil, and land surface data were collected from multiple remote sensing and ancillary sources and served as the independent variables. Specifically, elevation, slope, drainage density, geomorphology, topographic wetness index, and curvature maps were derived from the Shuttle Radar Topography Mission (SRTM) Digital Elevation Model (30 m × 30 m resolution) downloaded from the United States Geological Survey (USGS) Earth Explorer and processed in ArcGIS 10.8.

The aeromagnetic data were analyzed for subsurface lineament density and depth to fracture maps, lithological map was extracted from the 1:250,000 Geological Survey of Nigeria dataset, soil map from the Food and Agriculture Organization (FAO) database, and Surface lineament density and land use/land cover maps from Landsat-8 Operational Land Imager (OLI) imagery.

B. Generation of Thematic Layers and Evaluation of Aquifer Transmissivity

1. Generation of thematic layers

Twelve (12) thematic layers influencing groundwater occurrence were generated from geospatial and ancillary datasets within a GIS framework. They include: slope, elevation, drainage density, surface lineament density, geomorphology, land use/land cover, topographic wetness index (TWI), curvature, soil, lithology, subsurface lineament density, and depth to fracture maps. Topographic and hydrological parameters were generated from SRTM DEM, slope map from the *Slope* function in the Spatial Analyst toolbox of ArcGIS, elevation map from the DEM, and drainage networks from the DEM using Flow Direction and Flow Accumulation tools. Drainage density was subsequently computed by dividing the total stream length within each grid cell by its corresponding area (Rahmati et al, 2015; Naghibi et al, 2016).

The Curvature maps (plan and profile) were derived from the DEM using the *Surface Analysis* tool. These maps are used quantify terrain convexity and concavity, which influence surface runoff and infiltration patterns (Naghibi et al, 2016; Rahmati et al, 2015). Geomorphological units were delineated from satellite imagery via visual interpretation in addition with DEM-derived terrain models. To highlight landforms with differing groundwater recharge potential, the mapped features were digitized and rasterized within the GIS environment (Li et al., 2023; Naghibi et al., 2016). The Topographic Wetness Index (TWI) was computed using Equation (1).

$$TWI = ln\left(\frac{As}{tan\,\beta}\right) \qquad (1)$$

where As denotes the specific catchment area (flow accumulation), and β represents the slope gradient (Oso et al, 2026).

The analysis was implemented through the *Raster Calculator* and hydrological tools in ArcGIS. The geological map of the study area was sourced from the NGSA, scanned, georeferenced, and digitized in ArcGIS. Lithological units were vectorized and converted into raster format to capture the spatial variability of rock types and their groundwater potential (Rahmati et al, 2015; Adiat et al, 2020). Soil maps were obtained from the national soil survey database, georeferenced, digitized, and rasterized. Based on its texture and permeability characteristics, each soil unit was assigned a unique code to assess its role in infiltration and recharge potential (Rahmati et al, 2015; Naghibi et al, 2016).

Lineaments were extracted from Landsat-8 OLI data through both automatic and manual techniques. Directional and edge-enhancement filters were applied to emphasize linear features, which were later digitized and refined to exclude anthropogenic structures such as roads and pipelines. The lineament density map, which depicts the concentration of structural features that control groundwater movement, was generated using the Line Density tool in ArcGIS (Adiat et al, 2020; Rahmati et al, 2015). The land use/land cover (LULC) map was produced from Landsat-8 imagery using the supervised classification technique with the Maximum Likelihood Algorithm. Four major classes reflecting varying capacities for groundwater recharge were identified in the LULC map to include: built-up areas, vegetation, bare surfaces, and water bodies. The resulting map was imported into ArcGIS and converted to raster format for spatial integration (Adiat et al, 2020; Rahmati et al, 2015).

Aeromagnetic data from the Nigerian Geological Survey Agency (NGSA) were processed using Oasis Montaj software to apply filtering techniques that delineate subsurface structures controlling groundwater occurrence. To highlight fracture zones, the Total Magnetic Intensity (TMI) grid was reduced to the equator (RTE) and enhanced using Analytic Signal (AS), Total Horizontal Derivative (THD), First Vertical Derivative (FVD), and Tilt Derivative (TDR) filters. Euler Deconvolution provided depth estimates to magnetic sources, interpreted as fracture depths. The interpreted lineaments and Euler depth data were digitized and analyzed in ArcGIS to produce the subsurface lineament density and depth-to-fracture maps, respectively. All geospatial datasets were standardized to a uniform spatial resolution and projected to the Universal Transverse Mercator (UTM) Zone 31N coordinate system. The thematic layers were subsequently categorized using the natural breaks (Jenks) classification

method to ensure meaningful value grouping and minimize intra-class variation.

The depth-to-fracture map was derived using Euler deconvolution of the aeromagnetic dataset, with parameter selection guided by the geological characteristics of the Precambrian basement terrain typical of southwestern Nigeria. A structural index of 1 was adopted, which is appropriate for delineating linear features such as faults and fracture zones that dominate crystalline basement environments. The moving window size was selected to balance spatial resolution and solution stability, ensuring sufficient data points within each window while minimizing edge effects; this choice is consistent with established practices in regional-scale aeromagnetic interpretation. A tolerance level was applied to constrain the clustering of Euler solutions and filter out spurious depth estimates, thereby improving the reliability of the interpreted structural features.

The resulting depth solutions were qualitatively validated through comparison with available subsurface information, including VES-derived layer thicknesses and borehole lithologs within the study area. The correspondence between shallow to intermediate Euler depths and weathered/fractured zones identified from geoelectrical sounding supports the reliability of the interpretation. This integrated approach is consistent with previous studies in basement complex terrains of southwestern Nigeria, where aeromagnetic-derived structural information has been shown to correlate well with hydrogeologically significant fracture systems.

2. Evaluation of aquifer transmissivity

Transmissivity, a key hydrogeological parameter for evaluating aquifer productivity, was derived from the interpreted VES data. Field measurements were obtained using the Schlumberger electrode configuration, which is effective for delineating layered subsurface structures in crystalline terrains. Preliminary interpretation of the VES curves was carried out through manual curve matching to obtain initial estimates of layer resistivities and thicknesses. These preliminary models were further refined and inverted using the WinRESIST software to generate more accurate geoelectric parameters. The interpreted layer resistivities and thicknesses reflect the electrical and hydraulic properties of the subsurface materials.

Hydraulic conductivity (K) and transmissivity (T) were estimated from the geoelectric parameters (formation resistivity and aquifer thickness) derived from the interpreted VES data. Hydraulic conductivity (K) for each VES location using the empirical relationship established by Heigold et al (1979**)**, as expressed in Equations (2) and (3), respectively (Adiat et al, 2020). This indirect approach provides a reliable means of estimating aquifer transmissivity in the absence of direct pumping test data. The derived transmissivity values were later used as the dependent variable in the probabilistic frequency ratio model to establish relationships between subsurface hydraulic properties and spatially distributed groundwater-conditioning factors.

$$K = 386.4\, R^{-0.93283} \qquad (2)$$

where R is the resistivity

$$T = K\, h \qquad (3)$$

where K is the hydraulic conductivity and h is the aquifer thickness.

The Heigold-type empirical resistivity–transmissivity relationship relates aquifer resistivity to hydraulic properties through a power-law function. Although originally developed for unconsolidated sedimentary environments, this approach is widely applied in basement complex terrains such as Ekiti State in southwestern Nigeria, due to its operational practicality. In these settings, the development of deep weathering horizons, intense fracturing, and interconnected lineaments creates secondary porosity systems that hydrogeologically mimic classic sedimentary frameworks. Nevertheless, because it relies on transferring a primary-porosity model to a fractured crystalline terrain, this approach inherently carries structural uncertainties associated with empirical model fitting.

The original formulation reports a correlation coefficient (R^2) indicative of moderate to strong agreement, alongside a measurable standard deviation in residuals, reflecting natural variability in subsurface conditions. Consequently, the derived hydraulic conductivity and transmissivity values should be interpreted as approximate estimates rather than exact representations. Although full uncertainty propagation was not undertaken to avoid over-parameterization of the model, the adopted transmissivity threshold (15 m²/d) remains sufficiently robust within the expected range of variability. This is supported by the consistency observed between model predictions and independent borehole validation data, suggesting that the empirical uncertainty does not significantly affect the overall groundwater potential classification.

The computed transmissivity values were then screened and categorized into effective and non-effective points based on thresholds modified from Offodile (1983) (Table 1). Model accuracy was improved to better represent the spatial variability of aquifer productivity, by logarithmically subdividing Offodile's transmissivity range (5–50 m²/d) originally designated as "low" potential into two subclasses: low (5–15 m²/d) and low–moderate (15–50 m²/d)**.**

Considering the fact that small variations in transmissivity can significantly affect groundwater yield, this approach enhances the Frequency Ratio (FR) model's resolution by differentiating between poorly productive and marginally productive aquifers (Heigold et al., 1979). Consequently, only VES points with transmissivity values ≥ 15 m²/d, were classified as *effective* and used for modeling, while those with values < 15 m²/d were considered *non-effective* and excluded due to their minimal predictive relevance. The 15 m²/d threshold corresponds approximately to the lower quartile of transmissivity distribution and aligns with moderate-yield basement aquifers reported in recent regional studies (Oso et al., 2026).

Table 1 Aquifer Classification Based on Transmissivity Values (Offodile, 1983)

Transmissivity (m^2/d)	Potential for Groundwater
> 500	High
50–500	Moderate
5–50	Low
0.5–5	Very low
< 0.5	Negligible

C. Groundwater potential modeling using the Frequency Ratio technique

1. Derivation of FR for classes within the thematic layers

The Frequency Ratio (FR) model is a bivariate statistical approach that evaluates the spatial relationship between a dependent variable (transmissivity) and multiple independent thematic factors such as lithology, slope, land use/land cover, drainage density, etc. (Naghibi et al, 2016; Rahmati et al, 2015; Das and Pardeshi, 2018). With this method, the degree of influence that each factor exerts on the occurrence or distribution of the dependent variable is being quantified. In this approach, VES locations classified as effective based on transmissivity thresholds were converted into a point shapefile in ArcGIS and subsequently overlaid on each thematic map to extract their spatial correspondences. The Frequency Ratio for each class within a thematic layer was then computed as the ratio between the proportion of groundwater-effective points occurring within that class and the proportion of the total area occupied by the same class across the study area. This ratio reflects the relative contribution or likelihood of each factor class to groundwater occurrence. Mathematically, the FR can be expressed as shown in Equation (4).

$$FR = \frac{(\text{N\_sub} / \text{N\_total})}{(\text{A\_sub} / \text{A\_total})} \quad (4)$$

where N_sub is the number of effective VES points in a class, N_total is the total number of effective VES points, A_sub is the area of the class, and A_total is the total area of the study region.

The FR model was implemented as a binary classification problem, where transmissivity ≥15 m²/d represents effective groundwater zones. Positive spatial association, implying that groundwater occurrence is more likely within that particular class is signified by a Frequency Ratio (FR) value greater than one (FR > 1). Conversely, an FR value less than one (FR < 1) denotes a weaker or negative relationship, suggesting limited groundwater potential. The computed FR values for each class were subsequently used as weights in their corresponding thematic layers, reflecting the relative contribution of each factor to groundwater occurrence.

Widely recognized for its analytical simplicity, transparency, and reproducibility, the FR model relies entirely on empirical spatial data rather than subjective judgment or expert-based weighting (Li et al., 2023; Rahmati et al, 2015). The Frequency Ratio (FR) values represent the relative influence of each class within the thematic factors on the occurrence of groundwater. After computing the FR for all classes in each thematic layer, these values were applied as weights to their corresponding raster classes. The weighted thematic maps were subsequently integrated in the GIS environment through a cell-by-cell summation of the FR scores across all layers, producing a Groundwater Potential Prediction Index (GwPPI).

2. Integration of Frequency Ratio–Weighted Thematic Layers

The weighted thematic layers were integrated within a GIS framework to produce the groundwater potential prediction map of the study area. Each thematic factor was assigned a weight based on its relative importance in influencing groundwater occurrence, as derived from the Frequency Ratio (FR) model. The weighted linear combination (WLC) method was applied to ensure proportional representation of each factor in the final composite map. In this composite raster, each pixel value represents the cumulative FR contribution from all conditioning factors, with higher values signifying areas of greater groundwater potential. The integration process is mathematically expressed as Equation (5).

$$GwPPI = \sum FR_i \quad (5)$$

where i = 1, 2, 3, …, 12

The individual classes within each layer were normalized and reclassified according to their FR values, ensuring consistency in scale and comparability across datasets. Subsequently, all weighted and standardized layers were integrated using the raster calculator tool in ArcGIS to generate the final GwPPI map by applying Equation (5). The resulting output delineated the study area into distinct GPZs, ranging from very low, low, moderate to high potential using the Natural Breaks (Jenks) classification method to ensure optimal distinction between categories of similar statistical properties (Jenks, 1967; Rahmati et al, 2015).

D. Validation of the groundwater potential map using borehole yield data

Quantitative validation was employed to ensure the reliability of the generated groundwater potential prediction map. Borehole yield data of fifteen (15) existing boreholes, within the study area, were obtained from the Ekiti State Rural Water Supply and Sanitation Agency (EK-RUWASSA) and Geo-electric Shore Consult Nigeria Limited for this purpose. The borehole locations were converted into point shapefiles and overlaid on the predicted GPM to evaluate the correspondence between observed borehole yields and the model-predicted zones using Table 2 as a reference.

Table 2 Groundwater Yield Classification for Domestic Water Supply

Discharge (L/s)	Borehole yield (m^3/d)	Suitability description	Class	Reference
< 0.1	< 8.6	Insufficient – unlikely to meet household needs	Very low	Driscoll, 1986
0.1–0.3	8.6–26	May support a small household, close to the WHO minimum demand	Low	Todd and Mays, 2005; WHO, 2022
0.3–1.0	26–86	Adequate for typical households and small groups	Moderate	Driscoll, 1986
> 1.0	> 86	Reliable for multiple households, communities, and small-scale irrigation	High	Todd and Mays, 2005

The predictive performance of the groundwater potential models was evaluated using the Receiver Operating Characteristic (ROC) curve analysis based on borehole validation data. A structured threshold-based classification scheme was adopted, ranging from very low to high groundwater potential classes. The classified groundwater potential zones were re-grouped into binary outcomes. Moderate-to-high potential zones were considered productive (1), whereas low and very low zones were classified as non-productive (0). The confusion matrix parameters, including true positives (TP), false positives (FP), true negatives (TN), and false negatives (FN), were computed at multiple threshold levels (Table 3).

To ensure proper ROC representation, the analysis incorporated a baseline condition in which no locations were classified as groundwater potential zones, thereby establishing the origin point (0,0). Similarly, the terminal condition corresponds to a scenario in which all locations are classified as positive, i.e., (1,1).

Table 3 ROC Parameters for GwPPM

Threshold Condition	TP	FP	FN	TN	TPR	FPR
No positive prediction	0	0	9	6	0.000	0.000
≥ 4.0	1	1	8	5	0.111	0.167
≥ 3.5	2	1	7	5	0.222	0.167
≥ 3.0	6	3	3	3	0.667	0.500
≥ 2.5	7	4	2	2	0.778	0.667
≥ 2.0	8	5	1	1	0.889	0.833
≥ 1.5	9	6	0	0	1.000	1.000
≥ 1.0	9	6	0	0	1.000	1.000

IV. RESULTS AND DISCUSSION

A. Statistical Analysis of Effective and Non-Effective Aquifer Transmissivity

Statistical analysis of the transmissivity data (Table 4) justified the use of effective VES points only in Frequency Ratio (FR) modeling. Out of the 150 VES locations evaluated, 88 stations exhibited transmissivity values exceeding the 15 m^2/d threshold. Within these higher-yielding locations, transmissivity ranged from 15.01 to 318.04 m^2/d, with a calculated mean of 53.27 m^2/d. They are values of moderate to high groundwater potential aquifers. On the other hand, when non-effective points were considered, the overall mean transmissivity dropped to 33.86 m^2/d, mainly because most of those points were under 1 m^2/d, which represents unproductive or hydrogeologically insignificant areas.

This comparison reveals that low-transmissivity points skew the statistical representation of the aquifer system thereby lowering the model's accuracy. Using only effective points therefore ensures that the FR model is derived from data that reflects actual groundwater potential. This approach enhances both the reliability and predictive strength of the groundwater potential prediction map, in line with earlier studies emphasizing the exclusion of low-yielding data to improve hydrogeological modeling accuracy (Krasny, 1993; Todd and Mays, 2005).

Table 4 Statistics for Aquifer Parameters

VES Category	Statistics	Aquifer Resistivity (Ωm)	Aquifer Thickness (m)	Hydraulic Conductivity (m/d)	Transmissivity (m²/d)
Effective VES (88 Points)	Min	5.30	1.20	0.51	15.01
	Max	1212.50	42.70	81.55	318.04
	Mean	222..54	13.04	6.42	53.27
	Std Dev.	228.43	9.09	9.75	54.81
Non-effective VES (62 points)	Min	73.10	0.90	0.04	0.12
	Max	17275.10	33.70	7.05	14.84
	Mean	1691.90	7.29	1.34	6.31
	Std Dev.	3396.22	7.17	1.32	4.37
All VES (150 points)	Min	5.30	0.90	0.04	0.12
	Max	17275.10	42.7	81.55	318.04
	Mean	829.87	10.64	4.29	33.86
	Std Dev.	2253.64	8..85	7.93	48.17

Although only 88 of the 150 VES points were retained for model training based on the transmissivity threshold (≥15 m²/d), their spatial distribution was examined to ensure representativeness. The selected and excluded points are not confined to specific lithological or geomorphic units but are distributed across the study area, indicating the absence of significant spatial clustering. The excluded low-transmissivity points occur intermittently within the same hydrogeological settings as the retained data, thereby reducing the likelihood of systematic spatial bias. This probabilistic normalization minimized the influence of uneven spatial sampling by emphasizing aquifer productivity rather than sample density, thereby producing a more robust and hydrogeologically representative groundwater potential model. The reliability of this approach is supported by validation against independent borehole data.

B. Application of the Frequency Ratio Model for Groundwater Potential Assessment

1. Frequency ratio computation for thematic layers

The FR evaluation was based on the ratio of the probability of effective aquifer transmissivity occurrence in each class to the probability of that class within the total study area. The effective VES points, were therefore georeferenced and spatially overlaid on each thematic layer (Figures 3–14) to compute the FRs (Table 5) and quantify the degree of association between groundwater-yielding locations and the controlling hydrogeological, topographic, and structural factors governing groundwater occurrence in the study area.

Figures 3–14 collectively depict the spatial variability of key groundwater conditioning factors within the study area. The elevation map (Figure 3) reveals topographic variation that influences runoff and recharge distribution, while the slope map (Figure 4) highlights predominantly gentle slopes that favor infiltration over surface flow. The drainage density map (Figure 5) indicates zones of low to moderate drainage, suggesting enhanced infiltration capacity in less dissected areas. Geomorphological units (Figure 6) further delineate plains and undulating terrains that support groundwater accumulation. The Topographic Wetness Index (Figure 7) identifies moisture-convergent zones with high recharge potential, whereas the curvature map (Figure 8) distinguishes concave and convex landforms that control water accumulation and dispersion. Structural influences are evident in both the surface lineament density (Figure 9) and subsurface lineament density map, which highlight fracture-controlled pathways for groundwater movement and storage. Anthropogenic and natural surface characteristics are represented in the land use/land cover map (Figure 10), showing vegetation-dominated areas that enhance infiltration. Subsurface controls are further defined by the lithology map (Figure 11), indicating rock types with varying degrees of weathering and fracturing, and the soil texture map (Figure 12), where permeable soils promote recharge. The Subsurface lineament density map (Figure 13) further refines structural influence at the surface scale and captures deeper fracture systems that significantly control groundwater storage and flow in basement terrains. Finally, the depth to fracture map (Figure 14) identifies zones with deeper weathered/fractured layers that are favorable for groundwater accumulation, collectively providing an integrated basis for groundwater potential assessment.

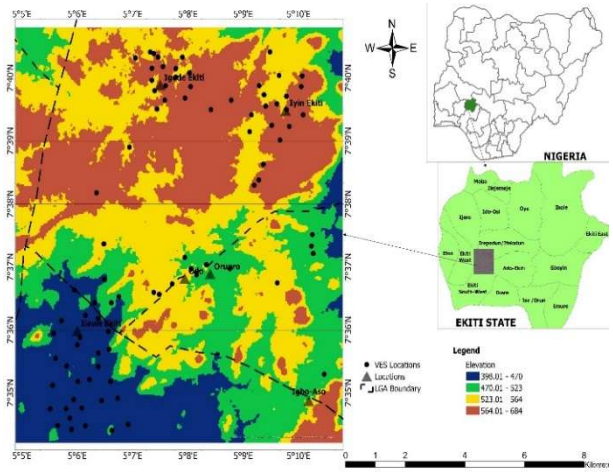

Figure 3 Elevation map (Oso et al., 2026)

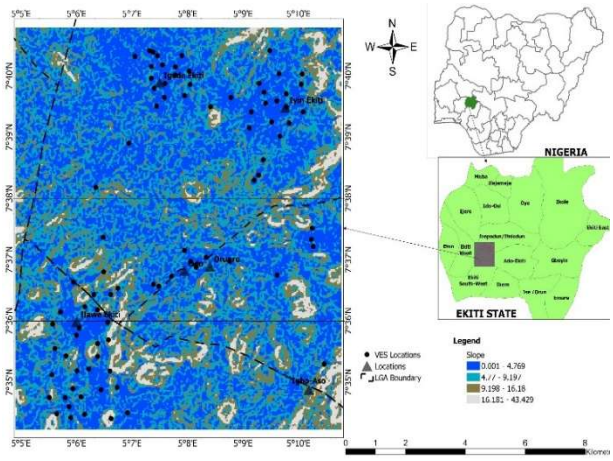

Figure 4 Slope map (Oso et al., 2026)

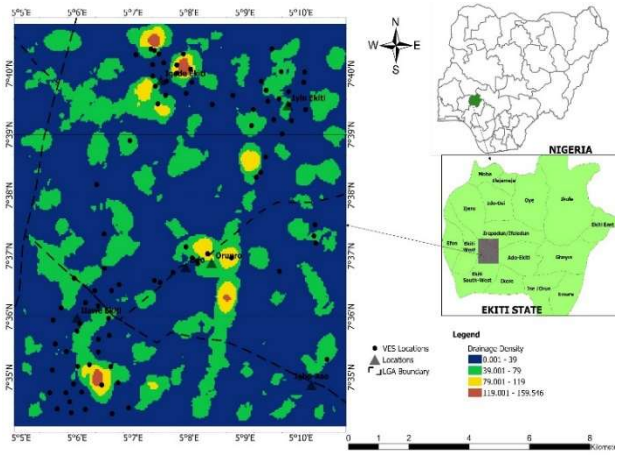

Figure 5 Drainage Density map (Oso et al., 2026)

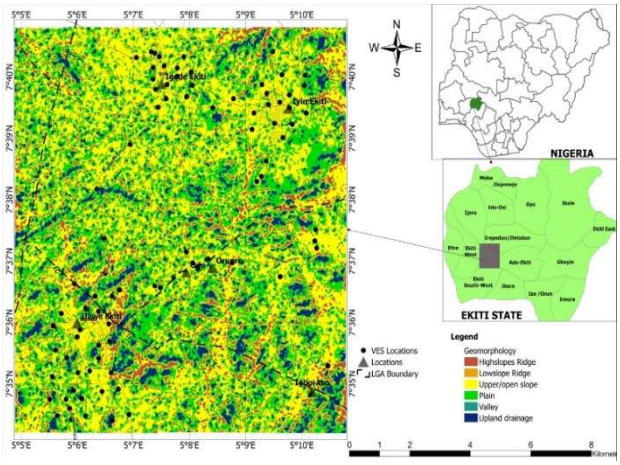

Figure 6 Geomorphology map (Oso et al., 2026)

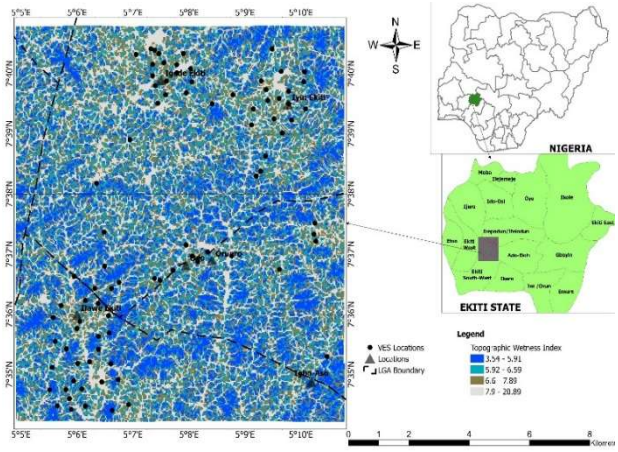

Figure 7 Topographic Wetness Index map (Oso et al., 2026)

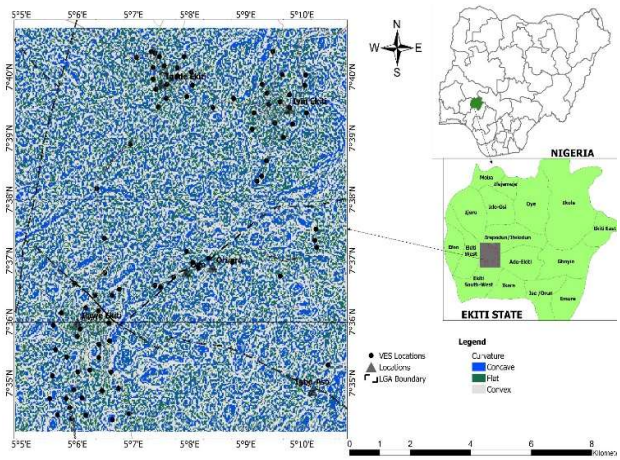

Figure 8 Curvature map (Oso et al., 2026)

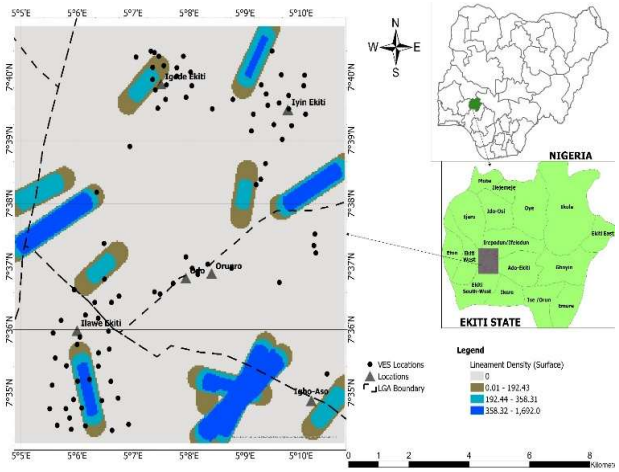

Figure 9 Surface Lineament Density map (Oso et al., 2026)

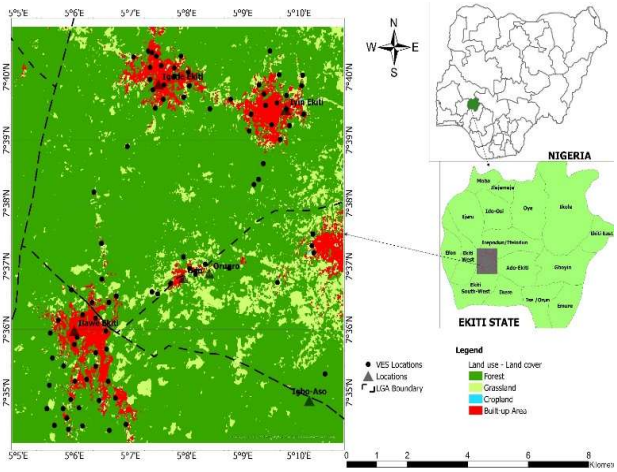

Figure 10 Land Use/Land Cover map (Oso et al., 2026)

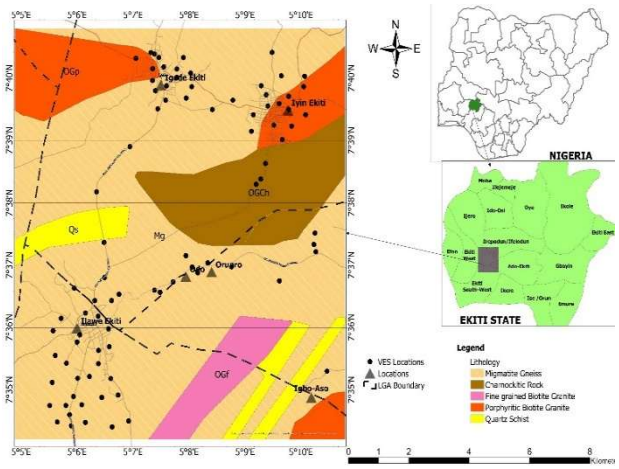

Figure 11 Lithology map (Oso et al., 2026)

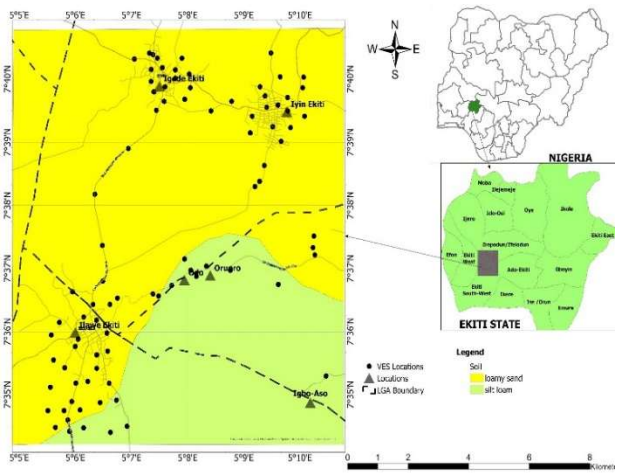

Figure 12 Soil Texture map (Oso et al., 2026)

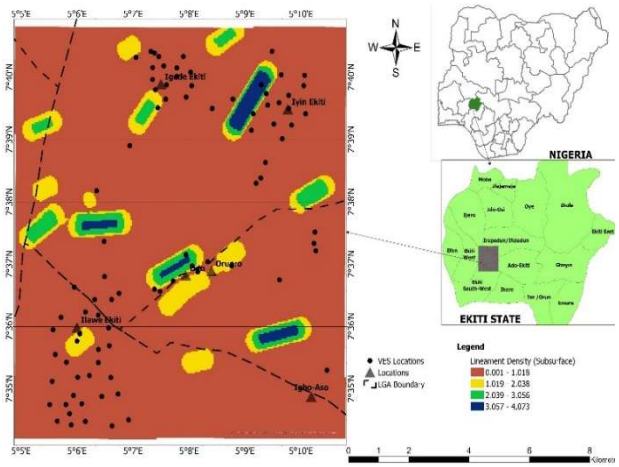

Figure 13 Subsurface Lineament Density map (Oso et al., 2026)

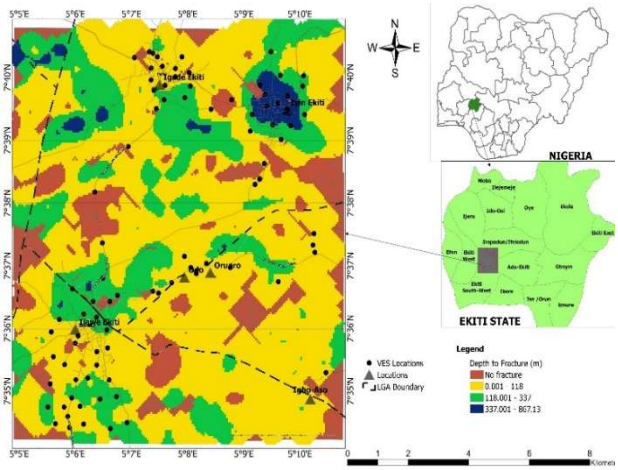

Figure 14 Depth to Fracture map (Oso et al., 2026)

Table 5 Computed Frequency Ratios for Thematic Layers

S/N	Thematic Factors	Classes	Area (%) (A)	Effective VES (N_Sub)	Effective Probability (P_E) = (N_Sub / 88)	Freq. Ratio (Fr) = (P_E / A)
1.	Lithology	Charnockitic rock	11.03	3	0.0341	0.31
		Migmatite gneiss	68.11	38	0.4318	0.63
		Fine grained b/granite	4.42	37	0.4205	9.51
		Porphyritic b/granite	11.23	10	0.1136	1.01
		Quartz schist	5.21	0	0	0
2.	Lineament density (Surface) (km/km^2)	0	84.44	80	0.9091	1.08
		0.001–192.43	5.24	7	0.0795	1.52
		192.44 - 358.31	5.16	1	0.0114	0.22
		358.32 – 1692.0	5.16	0	0	0
3.	Lineament density (Sub-surface) (km/km^2)	0.001 – 1.018	89.18	76	0.8636	0.97
		1.019 – 2.038	6.38	9	0.1023	1.60
		2.039 – 3.056	3.10	2	0.0227	0.73
		3.057 – 4.073	1.34	1	0.0114	0.85
4.	Drainage density (km/km^2)	0 – 39	76.21	59	0.6704	0.88
		39.01 – 79	21.30	23	0.2614	1.23
		79.01 – 119	2.14	5	0.0568	2.65
		119.01 – 159.55	0.35	1	0.0114	3.26
5.	Geomorphology	Highslopes ridges	12.61	25	0.2841	2.25
		Lowslopes ridges	34.84	2	0.0227	0.07
		Upper/Open slopes	27.26	25	0.2841	1.04
		Plain	6.18	33	0.3750	6.07
		Valley	7.00	2	0.0227	0.32
		Upland drainages	12.11	1	0.0114	0.09
6.	Depth to fractures (m)	No fractures	5.88	0	0	0
		0.001 – 118	66.88	55	0.6250	0.93
		118.001 – 357	24.72	28	0.3182	1.29
		357.001 – 867.13	2.52	5	0.0568	2.25
7.	Slope (°)	0 – 4.77	42.56	42	0.4773	1.12
		4.78 – 9.2	36.37	35	0.3977	1.09
		9.21 – 16.18	15.71	8	0.0909	0.58
		16.19 – 43.43	5.36	3	0.0341	0.64
8.	Elevation (m)	398 – 470	17.01	30	0.3409	2.00
		471 – 523	22.38	10	0.1136	0.51
		524 – 564	33.48	23	0.2614	0.78
		565 - 684	27.13	25	0.2841	1.05
9.	Soil texture	Silty loam	28.98	14	0.1591	0.55
		Loamy sand	71.02	74	0.8409	1.18
10.	Land use/land cover	Forest cover	82.37	33	0.3750	0.46
		Grassland	10.80	15	0.1705	1.58
		Cropland	0.06	0	0	0
		Built-up	6.77	40	0.4545	6.71
11.	Topographic Wetness Index	3.53 – 5.91	24.90	16	0.1818	0.73
		5.92 – 6.59	24.69	14	0.1591	0.64
		6.60 – 7.89	26.59	34	0.3864	1.45
		7.90 – 20.89	23.82	24	0.2727	1.14
12.	Curvature	Concave	23.25	18	0.2045	0.88
		Flat	26.99	41	0.4659	1.73
		Convex	49.76	29	0.3295	0.66

2. Interpretation and integration of frequency ratio results

The FR results (Table 4) highlight the varying influence of each thematic factor on groundwater potential across the study area. In general, FR values greater than 1 denote favorable hydrogeological conditions, whereas values below 1 indicate low groundwater potential (Naghibi et al., 2016; Das and Pardeshi, 2018). Among the lithological units, fine-grained biotite granite (FR = 9.51) exhibits the strongest association with groundwater occurrence, followed by porphyritic biotite granite (FR = 1.01), while migmatite gneiss (FR = 0.63) shows a comparatively lower potential. The high FR values associated with the granitic rocks suggest that they have undergone significant weathering and fracturing, leading to enhanced secondary porosity and permeability (Todd and Mays, 2005; Offodile, 2002). Structural factors also play a key role, as moderate surface lineament density (192.44–358.31 km/km²; FR = 1.52) and subsurface lineament density (1.019–2.038 km/km²; FR = 1.60) correspond to increased groundwater potential. This observation aligns with previous studies emphasizing that moderate fracture intensity promotes recharge and groundwater storage (Adiat et al, 2020; Rahmati et al, 2015).

Geomorphological and drainage parameters further influence groundwater occurrence. Plains (FR = 6.07) represent the most favorable geomorphic units, reflecting high infiltration capacity, while high-slope ridges and uplands with lower FR values correspond to poor recharge zones. Similarly, low drainage density (0–39 km/km²; FR = 0.88) areas enhance infiltration by reducing surface runoff (Rahmati et al, 2015). Topographic and soil attributes also support recharge. Gentle slopes (0–4.77°; FR = 1.12) and moderately elevated areas (398–470 m; FR = 2.00) show strong groundwater associations. Loamy sand soils (FR = 1.18) and vegetated areas such as grassland and cropland (FR > 1.0) favor infiltration and percolation. Additionally, high Topographic Wetness Index (6.60–7.89; FR = 1.45) values correspond to moisture-convergent zones conducive to groundwater recharge (Pourghasemi and Beheshtirad, 2015). In summary, the FR model indicates that lithology, subsurface lineament density, geomorphology, and slope exert the strongest control on groundwater occurrence. Zones underlain by fractured granitic rocks, characterized by moderate subsurface lineament density, gentle slopes, and plains, represent the most promising areas for groundwater development.

The insights derived from the frequency ratio analysis formed the basis for generating the final groundwater potential prediction map (Figure 15). By integrating the weighted thematic layers using their respective FR values, areas with varying groundwater prospects were delineated. This integration highlights spatial patterns where favorable geological, structural, and topographic conditions converge to enhance groundwater occurrence. The resulting map, therefore, provides a realistic visualization of how the combined influence of these factors translates into distinct zones of groundwater potential across the study area.

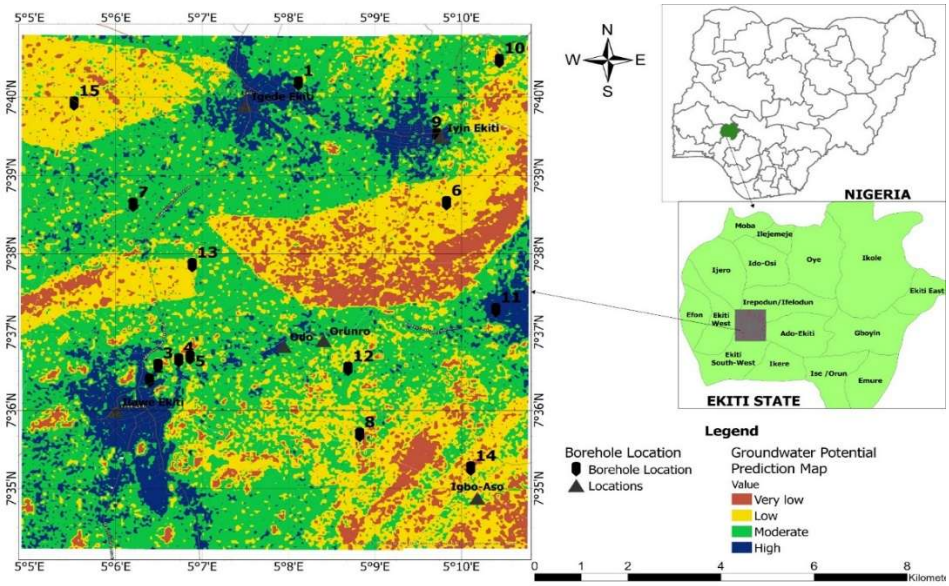

Figure 15 Groundwater Potential Prediction map

3. Assessment of the derived groundwater potential prediction map

The Frequency Ratio–based integration produced a groundwater potential prediction map (GwPPM) that categorizes the area into very low, low, moderate, and high potential zones (Figure 15). These classes represent the spatial variability of groundwater occurrence controlled by lithological, structural, topographic, and geomorphological factors. Quantitative analysis of the classified raster reveals that moderate potential zones dominate the study area, covering approximately 45.40% of the total surface area. Low potential zones accounted for about 30.17%, while high potential zones occupied roughly 13.08%. The remaining 11.35% of the area falls within the very low potential category.

This distribution indicates that about 58.48% of the area possesses moderate to high groundwater potential, emphasizing favorable hydrogeological conditions in several parts of the region. Spatially, high to moderate potential zones are mainly concentrated in the central and northern sectors, particularly around Igede-Ekiti and Iyin-Ekiti, where moderate lineament density, gentle slopes, and low drainage densities enhance infiltration and groundwater storage (Olomo et al, 2025; Nazaripour et al, 2024). These regions are typically underlain by fractured biotite granite and migmatite gneiss, which favor the development of secondary porosity and permeability (Todd and Mays, 2005).

Conversely, low to very low potential zones are predominant in the southern and southeastern regions, notably around Ilawe-Ekiti and Igbo-Aso. These zones coincide with rugged topography, high drainage density, and less fractured lithologies such as charnockitic rocks, which limit infiltration and increase surface runoff (Adiat et al, 2020; Ojo et al, 2021). The moderate potential zones occur as transitional belts, representing areas with mixed lithological and geomorphic settings that sustain moderate recharge (Rahmati et al, 2015; Das and Pardeshi, 2018).

Structurally, the delineated groundwater potential pattern corresponds closely with the regional NE–SW and E–W fracture orientations, which serve as principal groundwater conduits within the crystalline basement terrain. These fracture systems, interpreted from lineament density and orientation analysis, form interconnected pathways that enhance groundwater migration and storage, especially where they intersect. The concentration of high potential zones along these structural corridors underscores the critical role of tectonic fabrics in groundwater accumulation and flow dynamics within hard rock environments (Adiat et al, 2020; Chandra et al, 2019; Fernandes, 2023). Generally, the central and northern portions of the study area are the most promising for groundwater development, while southern areas display limited aquifer productivity due to structural and lithological constraints.

C. Validation of the Derived Map

Validation of the FR–derived Groundwater Potential Prediction Map (GwPPM) was conducted using borehole yield data from fifteen locations within the study area (Table 6). The comparison revealed a strong correspondence between the predicted potential zones and the observed borehole yields. Specifically, twelve boreholes (80%) showed a direct spatial match between mapped potential and measured discharge, whereas three (20%) exhibited partial or no agreement. Boreholes 9 and 15 located in high-potential zones recorded the highest yields, ranging from 1.11–1.50 L/s (95.9–129.6 m^3/d). These locations correspond to structurally controlled or deeply weathered aquifer zones, consistent with high groundwater accumulation potential. Similarly, boreholes within moderate to moderately high potential zones (e.g., boreholes 1–5, 7, and 12) showed yields between 0.32 and 1.00 L/s (27.65–86.40 m^3/d). This falls within areas characterized by moderate fracturing and weathering (Chandra et al, 2019; Lachassagne et al, 2021). In contrast, boreholes located within low to very low potential zones (e.g., boreholes 6, 8, 10, and 14) exhibited yields below 0.30 L/s (≤25 m^3/d), indicating poor groundwater potential. This is likely due to limited fracture connectivity or thin regolith development (Chandra et al, 2019; Lachassagne et al, 2021). However, a minor discrepancies were observed. Boreholes 13, and 15, which yielded moderate to high discharge values, were mapped within lower potential zones, and borehole 11 also deviated from the prediction map. Such deviations likely stem from localized subsurface variations, including fracture intersection points, micro-scale lithologic heterogeneity, or borehole construction influences not captured by regional-scale modeling (Chandra et al, 2019; Lachassagne et al, 2021).

Overall, the validation indicates that the FR-based groundwater potential model achieved approximately 80% accuracy, confirming its effectiveness in predicting spatial groundwater productivity. The observed agreement between modeled and measured data supports the reliability and practical applicability of the FR approach in crystalline basement terrains. These findings align with previous studies that have validated FR-based models using borehole or well yield data (Naghibi et al, 2016; Das and Pardeshi, 2018; Rahmati et al, 2015), reaffirming the robustness of this method for groundwater potential assessment.

Table 6 Model Output Validation Table

S/N	Coordinates *Latitude and Longitude*	Discharge (L/s)	Borehole yield (m^3/d)	Remarks	Spatial Potential on GwPPM
1.	7.668050°N, 5.135228°E	0.50	43.20	Moderate	Moderate
2.	7.604797°N, 5.106512°E	1.00	86.40	Moderate-High	Moderate–High
3.	7.607902°N, 5.108122°E	0.40	34.56	Moderate	Moderate
4.	7.609074°N, 5.112135°E	0.75	64.80	Moderate	Moderate
5.	7.609702°N, 5.114319°E	0.50	43.20	Moderate	Moderate
6.	7.642537°N, 5.163816°E	0.10	8.64	Very low–Low	Low
7.	7.642195°N, 5.103348°E	0.32	27.65	Low–Moderate	Moderate
8.	7.59322°N, 5.147058°E	0.29	24.69	Low	Low
9.	7.657092°N, 5.161916°E	1.50	129.60	High	High
10.	7.672844°N, 5.17401°E	0.10	8.64	Very low–Low	Low
11.	7.619763°N, 5.173318°E	0.20	17.28	Low	High
12.	7.607262°N, 5.144812°E	0.32	27.65	Low–Moderate	Moderate
13.	7.629352°N, 5.114751°E	1.25	108.00	High	Low
14.	7.586027°N, 5.168481°E	0.32	27.65	Low–Moderate	Low-Moderate
15.	7.66377°N, 5.091945°E	1.11	95.90	High	Low

The ROC curve (Figure 16) was generated by plotting the True Positive Rate (TPR) against the False Positive Rate (FPR) across the defined thresholds. The resulting curve indicates that the GwPPM model exhibits acceptable predictive capability, with the Area Under the Curve (AUC) value calculated as 0.71.

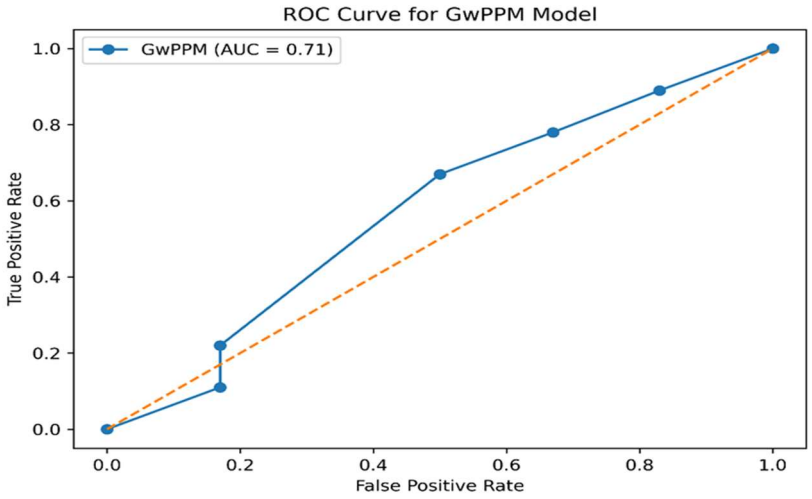

Figure 16 ROC Curve for GwPPM Model

D. Model Evaluation and Practical Implications

The transmissivity-constrained FR model employed herein provided a uniform spatial evaluation of groundwater potential in a crystalline basement terrain. Selecting only productive VES data with transmissivity above 15 m²/d (88 out of 150) enhanced the model predictive power to identify hydraulically productive aquifers. This screening increased the statistical stability of the analysis because the effective dataset recorded transmissivity values ranging from 15.01 to 318.04 m²/d with a mean of 53.27 m²/d, confirming moderate to high aquifer productivity. These threshold-based approaches have already been proven to improve the credibility of groundwater modeling by eliminating hydrogeologically meaningless zones (Pourghasemi and Beheshtirad, 2015; Das and Pardeshi, 2018).

The FR analysis revealed lithology and structural features with maximum control over groundwater occurrence (Moshe and Beza, 2024; Rahim et al, 2025). Porphyritic and fine-grained biotite granites with FR values of 9.51 and 1.01, respectively, contained maximum groundwater potential due to wide fracturing and weathering, which enhance secondary porosity and permeability. Migmatite gneiss (FR = 0.63) had the lowest potential. Moderate subsurface (1.019–2.038 km/km²) and surface (192.44–358.31 km/km²) lineament densities, equivalent to FR values of more than 1, also indicate that moderately fractured areas are favorable for infiltration and storage. This is in line with previous findings in comparable basement terrain (Adiat et al, 2020). Dominance of NE–SW and E–W fracture orientations also favors the structural influence of tectonic fabrics on groundwater migration and storage (Chandra et al, 2019; Fernandes, 2023). Topography and geomorphic status strongly regulate recharge distribution. Plains (FR = 6.07) and sloping land forms (0–4.77°; FR = 1.12) were confirmed suitable for recharging due to high infiltration and low runoff, whereas steep ridges and intensively dissected terrain yielded low groundwater potential. Low drainage density (0–39 km/km²; FR = 0.88) belts, loamy sand (FR = 1.18) soil, and vegetative land uses (FR > 1.0) boost recharging due to high infiltration and water storage. High Topographic Wetness Index (6.60–7.89; FR = 1.45) values associated with regions of convergent moisture supported recharge (Rahmati et al, 2015; Naghibi et al, 2016).

The FR model classified the study area into four groundwater potential zones: very low (11.35%), low (30.17%), moderate (45.40%), and high (13.08%). This indicates that approximately 58.48% of the study zone is having moderate to high potential. These favorable areas are located predominantly in the central and northern parts, particularly around Igede-Ekiti and Iyin-Ekiti, where there is a mixture of fractured granitic rocks, moderate structural density, and gentle topography. Conversely, the low to very low potential zones in the southern and southeastern areas (Ilawe-Ekiti and Igbo-Aso) are associated with rugged relief, high density of drainage, and massive charnockitic lithologies that are resistant to infiltration. The transmissivity values validation with borehole yield data confirmed the efficacy of the model. Twelve out of fifteen boreholes (80%) spatially overlapped with their mapped classes of potential, with high-potential zones yielding 1.11–1.50 L/s and low-potential zones yielding below 0.30 L/s. Local subsurface variations or construction variations not recorded at regional scale accounted for the small variations. The validation accuracy (≈80%) agrees with the previous FR-based groundwater modeling studies (Naghibi et al, 2016; Das and Pardeshi, 2018), re-affirming the efficiency of the transmissivity-based FR approach in groundwater potential mapping of crystalline basement rocks.

From the ROC Curve (Figure 16), the calculated AUC of 0.71 shows that the GwPPM model exhibits acceptable predictive capability. This value indicates moderate performance for the GwPPM model. To assess the uncertainty associated with these estimates, 95% confidence interval was computed using bootstrap resampling, and the model yielded a confidence interval of 0.57–0.85 which shows that the model exhibit a predictive performance well above random classification (0.50). Notwithstanding the satisfactory performance of the model, certain limitations should be acknowledged. First, the estimation of hydraulic conductivity using the Heigold et al. empirical relationship introduces inherent uncertainty, as such formulations are site-dependent and may not fully capture local subsurface variability. Second, the present model is static and does not explicitly incorporate temporal variations in groundwater recharge, such as seasonal rainfall fluctuations, which may influence groundwater availability over time.

Third, the use of a 30 m resolution DEM may not adequately resolve fine-scale fracture networks that significantly control groundwater occurrence in basement terrains. Finally, anthropogenic factors, including groundwater abstraction and land use changes, were not considered, although they can substantially modify recharge and storage conditions. These limitations suggest that the results should be interpreted as a regional-scale assessment and, where necessary, complemented with detailed site-specific investigations.

V. CONCLUSION

This study successfully applied a transmissivity-constrained Frequency Ratio (FR) model integrated in a GIS environment to delineate groundwater potential zones within a crystalline basement terrain. By imposing a transmissivity threshold of 15 m²/d, only 88 out of the 150 VES points were classified as hydraulically effective and retained for modeling. This refinement ensured that the derived groundwater potential prediction map was based on aquifers of true hydrogeological significance, thereby improving model precision and interpretive reliability. The FR-based analysis demonstrated that lithology, lineament density, geomorphology, slope, and topographic wetness are the principal factors controlling groundwater occurrence in the study area. The model revealed that about 58.48% of the total area falls within moderate to high GPZs, while 30.17% and 11.35% correspond to low and very low potential zones, respectively. Spatially, central and northern regions (notably Igede-Ekiti and Iyin-Ekiti) exhibit favorable hydrogeological conditions due to the dominance of fractured granitic rocks, moderate structural density, gentle slopes, and low drainage densities. In contrast, southern and southeastern sectors (Ilawe-Ekiti and Igbo-Aso) show limited potential,

reflecting the effects of rugged terrain, dense drainage, and less fractured lithologies such as charnockite.

Model validation using borehole yield data yielded an accuracy of approximately 80%, confirming the strong predictive performance of the FR technique in identifying productive groundwater zones. Deviations between predicted and observed results were attributed to localized fracture intersections and micro-scale lithological heterogeneities not captured by the regional-scale analysis. In summary, the FR-based GwPPM improves drilling success relative to random siting but should be used alongside conventional hydrogeological investigations.

Future studies should integrate dynamic hydro-environmental variables such as recharge rate, soil permeability, and seasonal water table fluctuations to enhance the temporal robustness and predictive accuracy of groundwater potential assessments. Implementing these measures will strengthen groundwater development planning and promote sustainable utilization of the resource across the region.

AUTHOR CONTRIBUTIONS

O.O. Oso: conceived and managed the project, designed the research, carried out field data collection, processed data, prepared the figures and tables, edited and approved the final draft; **O.S. Ogungbemi:** supervision, assisted with research design, analysis, and report review; **O.O. Afolabi**: co-supervision, assisted with research design, analysis, and report review; **H. O. Aliu**: reviewed and edited the draft manuscript.

ACKNOWLDGEMENT

The authors wish to extend their sincere gratitude to the Dean of the School of Engineering, the Head of Department, and the faculty members of the Department of Mineral and Petroleum Resources Engineering at the Federal Polytechnic, Ado-Ekiti, for their invaluable support throughout the course of this program.

REFERENCES

Adiat, K. A. N.; Ajayi, O. F.; Akinlalu, A. A. and Tijani, I. B. (2020). Prediction of groundwater level in basement complex terrain using artificial neural network: a case of Ijebu-Jesa, southwestern Nigeria. Applied Water Science, 10(1), 8. https://link.springer.com/article/10.1007/s13201-019-1094-6. SpringerLink.

Ojo, A. S.; Abam, T. K. S.; Tamunobereton-Ari, I. and Amakiri, A. R. C. (2021). Hydrogeological and Geophysical Investigation of Ground Water Potentials in Basement Terrain of Ado Ekiti, Southwestern Nigeria. IOSR Journal of Applied Geology and Geophysics 9(4): 11–25. https://iosrjournals.org/iosr-jagg/papers/Vol.%209%20Issue%204/Ser-2/B0904021125.pdf.

Chandra, S.; Auken, E.; Maurya, P. K.; Ahmed, S. and Verma, S. K. (2019). Large scale mapping of fractures and groundwater pathways in crystalline hardrock by AEM. Scientific Reports, 9 (1), 398. https://doi.org/10.1038/s41598-018-36153-1.

Das, S. and Pardeshi, S. D. (2018). Integration of different influencing factors in GIS to delineate areas using IF and FR techniques: a study of Pravara basin, Maharashtra, India. Applied Water Science, 8 (7), 197. https://doi.org/10.1007/s13201-018-0848-x

Driscoll, F.G. (1986). Groundwater and wells (2nd ed.). Johnson Filtration Systems.

Fernandes, A. J. (2023). Structural geology applied to fractured aquifer characterization. Groundwater Project. https://doi.org/10.21083/978-1-77470-009-9

Heigold, P. C.; Gilkeson, R. H.; Cartwright, K. and Reed, P. C. (1979). Aquifer transmissivity from surficial electrical methods. Ground Water, 17 (4): 338–345. https://doi.org/10.1111/j.1745-6584.1979.tb03325.x

Ibrahim, E. S., Chiroma, J. T., Abubakar, M. A., Ojih, S. A., Waziri, E. S., Daffi, R. E., & Yenne, E. (2024). Spatial modelling of present and future groundwater potentials in Nigeria; towards a sustainable water demand and supply. Sustainable Water Resources Management, 10(4), 137. https://doi.org/10.1007/s40899-024-01107-1

Ige, O. O.; Ameh, H. O. and Olaleye, I. M. (2021). Borehole inventory, groundwater potential and water quality studies in Ayede Ekiti, Southwestern Nigeria. Discover Water, 1 (1), 2. https://link.springer.com/article/10.1007/s43832-020-00001-z.

Jenks, G. F. (1967). The data model concept in statistical mapping. International Yearbook of Cartography, 7, 186–190.

Jha, R., Singh, V. P., Singh, V., Roy, L. B., & Thendiyath, R. (2022). Groundwater and water quality. Springer, London.

Krásný, J., (1993). Classification of transmissivity magnitude and variation. Groundwater, 31(2), pp.230-236, Dublin, Ohio.

Lachassagne, P.; Dewandel, B. and Wyns, R. (2021). Hydrogeology of weathered crystalline/hard-rock aquifers—guidelines for the operational survey and management of their groundwater resources. Hydrogeology Journal, 29 (8): 2561-2594. https://doi.org/10.1007/s10040-021-02339-7

Li, Y., Abdelkareem, M., & Al-Arifi, N. (2023). Mapping potential water resource areas using gis-based frequency ratio and evidential belief function. Water, 15(3), 480. https://doi.org/10.3390/w15030480

MacDonald, A. M.; Bonsor, H. C.; Dochartaigh, B. É. Ó. and Taylor, R. G. (2012). Quantitative maps of groundwater resources in Africa. Environmental Research Letters, 7 (2), 024009.

Moshe, A. and Beza, M. (2024). Assessment of groundwater potential zones using GIS-based multicriteria decision analysis: a case study on Enemor and Ener Woreda, Central Ethiopia Region. H2Open Journal, 7 (3): 286-302. https://doi.org/10.2166/h2oj.2024.020

Naghibi, S. A.; Pourghasemi, H. R. and Dixon, B. (2016). GIS-based groundwater potential mapping using boosted regression tree, classification and regression tree, and random forest machine learning models in Iran. Environmental monitoring and assessment, 188 (1), 44. https://opus.lib.uts.edu.au/bitstream/10453/130841/4/Manuscript%20Clean.pdf

Nazaripour, H.; Sedaghat, M.; Shafaie, V. and Movahedi Rad, M. (2024). Strategic assessment of groundwater potential zones: a hybrid geospatial approach. Applied Water Science, 14 (8), 185. https://doi.org/10.1007/s13201-024-02243-x

Offodile, M. E. (1983). The occurrence and exploitation of groundwater in Nigeria basement complex. Journal of Mining and Geology, 20 (1 & 2): 131–146.

Offodile, M. E. (2002). Ground water study and development in Nigeria. Mecon Geology & Eng. Services. https://www.scirp.org/reference/referencespapers?referenceid=2826344.

Olomo, O. K.; Danga, O. A. and Aliyu, A. O. (2025). Exploration of quality groundwater through lineament delineation in Okene and its surroudings. Geosystems and Geoenvironment, 4 (1), 100350. https://doi.org/10.1016/j.geogeo.2024.100350.

Oso, O. O., Ogungbemi, O. S., Afolabi, O. O., & Aliu, H. O. (2026). Groundwater potential mapping of the basement complex terrain of Ekiti State, Nigeria. Water Science, 40(1), 35. https://doi.org/10.1007/s44533-026-00037-5

Osumeje, J. O., Eshimiakhe, D., Oniku, A. S., & Lawal, K. M. (2024). Application of remote sensing and electrical resistivity technique for delineating groundwater potential in North Western Nigeria. Scientific reports, 14(1), 22299. https://doi.org/10.1038/s41598-024-69633-8

Oyedele, A. A.; Ayodele, O. S. and Olabode, O. F. (2019). Groundwater quality assessment and characterization of shallow basement aquifers in parts of ado ekiti metropolis, Southwestern Nigeria. SN applied Sciences, 1 (7), 669. https://link.springer.com/article/10.1007/s42452-019-0683-1.

Pourghasemi, H. R. and Beheshtirad, M. (2015). Assessment of a data-driven evidential belief function model and GIS for groundwater potential mapping in the Koohrang Watershed, Iran. Geocarto International. DOI: 10.1080/10106049.2014.966161.

Rahim, O. A.; Yin, H.; Ullah, S. and Durrani, A. N. (2025). Delineation of groundwater potential zones and recharge using multi-source big data and systematic analysis approach. Sustainable Futures, 100872. https://doi.org/10.1016/j.sftr.2025.100872

Rahmati, O.; Nazari Samani, A.; Mahdavi, M.; Pourghasemi, H. R. and Zeinivand, H. (2015). Groundwater potential mapping at Kurdistan region of Iran using analytic hierarchy process and GIS. Arabian Journal of Geosciences, 8 (9): 7059-7071. https://doi.org/10.1007/s12517-014-1668-4

Todd, D.K. and Mays, L.W. (2005). Groundwater hydrology (3rd ed.). John Wiley and Sons.

World Health Organization. (2022). Guidelines for drinking-water quality: fourth edition incorporating the first and second addenda. World Health Organization. https://www.who.int/publications/i/item/978924004506